Proceedings of the 17th World Congress
The International Federation of Automatic Control
Seoul, Korea, July 6-11, 2008

Virtual Decomposition Control of a Planar Flexible-Link Robot

Wen-Hong Zhu * **Christian Lange** * **Mathilde Callot** *

* *Spacecraft Engineering, Space Technologies, Canadian Space Agency*
6767 route de l'Aeroport, Saint-Hubert, QC, Canada J3Y 8Y9
(Tel: 450-926-5177; e-mails: Wen-Hong.Zhu@space.gc.ca,
Christian.Lange@space.gc.ca)

Abstract:
Use of flexible link robots is motivated by applications featuring lightweight or long arms. However, the control problem faces strong technical challenges resulting from the complex dynamics. In this paper, the *virtual decomposition control* (VDC) approach is applied for the first time to address the technical challenges of this thorny problem mainly resulting from the dynamic coupling effects among flexible links. In view of the VDC approach, the control problem of a multiple-flexible-link robot is no more complex than the control problem of individual flexible links subject to kinematics constraints. A planar beam governed by Euler-Bernoulli equation is studied as an example for simplicity. A possible extension to robots with multiple flexible links is theoretically possible by creating appropriate *virtual power flows* at the two ends of each beam. The validity of the theoretical results is verified by simulations with respect to two typical space systems in planar motion.

Keywords: Virtual decomposition control; Flexible arms; Robot control; End point control; Model-based control; Distributed-parameter systems; Partial differential equations.

1. INTRODUCTION

Control of flexible-link robots has been developed for more than two decades, see Kanoh et al. (1986). The research of this topic is crucial to robotic applications featuring lightweight or long arms. However, the resulting complex dynamics make development of efficient control algorithms highly challenging. While lightweight robot arms are always desirable due to cost advantages, long arms are needed for certain applications ranging from assembly tasks of the International Space Station (ISS) to aircraft cleaning tasks. However, when either lightweight or long arms are used, flexibility shows up inevitably regardless of the arm materials being used. This fact can be seen from the Euler-Bernoulli equation that the static deformation of a uniform cantilever beam subject to a force at the free end is proportional to the third power of the beam length. As a common practice in industry nowadays, robot controllers are generally based on lumped-parameter models. However, by restricting robot control design to rigid models, the operational efficiency is severally affected due to the extra time needed to damp out vibrations for safe task execution.

Unfortunately, the control of multiple-flexible-link robots has never been easy due to the complexity in deriving their dynamic equations that take into account the dynamic couplings among the multiple links. The use of distributed parameter models makes the dynamic equations of a multi-body system rather difficult, see Macchelli et al. (2007), and the development of control strategies quite complex, see Luo et al. (1999). By far, the most successfully designed controllers are either based on simplified models or limited to a rather small class of systems, see Junkins and Kim (1993), such as robots with one or two flexible beams in planar motion or robots with a specially designed mechanism or structure. In the early stage, an approximation based on finite-dimension models was applied by Wang and Vidyasagar (1992), and the dynamic inversion techniques were used by De Luca and Siciliano (1993). Luo (1993) examined strain-based feedback control. This research based the control on the Euler-Bernoulli equation with distributed-parameter in nature. Then, Queiroz et al. (1999) developed an adaptive controller to compensate for an unknown payload mass based on an infinite dimensional model of flexible-link robots. A careful literature review reveals that tracking control of multiple-flexible-link robots in three-dimension (3D) has not been well developed, besides a few specific cases on mechanical design and control (see Somolinos et al. (2002) and Khadem and Pirmohammadi (2003)).

In this paper, the *virtual decomposition control* (VDC) developed by Zhu et al. (1997) is applied for the first time to the tracking control problem of flexible link robots. In view of the VDC approach, only the dynamics of individual flexible links are required for constructing control laws, while the stability and convergence of the entire robot are guaranteed as long as the *virtual power flows* at the "cutting points" are appropriately handled.

This paper is organized as follows: the dynamic model of a planar flexible beam is given in Section 2. In Section 3, the model-based control law is presented together with the stability analysis, followed by appropriate handling of the *virtual power flows* at the two ends of the beam. Control

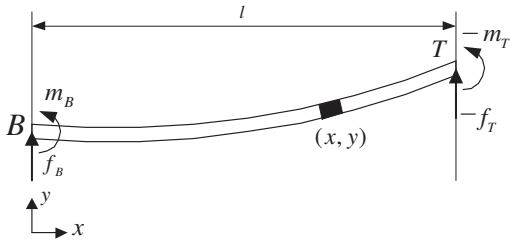

Fig. 1. A flexible link virtually decomposed from a planar flexible-link robot.

implementation is discussed in Section 4, and simulations using parameters from two typical space systems are demonstrated in Section 5.

2. FLEXIBLE LINK DYNAMICS

2.1 Flexible Link

An Euler-Bernoulli link virtually decomposed from a multiple-flexible-link robot is illustrated in Fig. 1.

This link is subject to following assumptions:

- The link is slender with uniform geometric and inertial characteristics.
- The link is flexible in the lateral directions and stiff with respect to axial forces and to axial torsion.
- The link has negligible shear deformation and negligible distributed rotational inertia.
- The link is restricted in a plane excluding the motion in x axis.
- No gravity is presented.

With respect to this link, two pairs of force and moment applied at both ends [1] are defined as

f_B	Shear force applied to the link at point B.
m_B	Bending moment applied to the link at point B.
f_T	Shear force applied from the link at point T.
m_T	Bending moment applied from the link at point T.

2.2 Extended Hamilton's Principle

Denote

$$K = \frac{1}{2}\int_0^l \rho \dot{y}(x,t)^2 dx \tag{1}$$

as the kinetic energy of the link and

$$V = \frac{1}{2}\int_0^l EIy''(x,t)^2 dx \tag{2}$$

as the potential energy of the link, where

l	Length of the link.
ρ	Mass per unit length.
E	Young's modulus of elasticity.
$I(x)$	Cross-sectional area moment of inertia of the link about its neutral axis.
$\dot{y}$	Partial derivative of $y(x,t)$ with respect to time t.
y'	Partial derivative of $y(x,t)$ with respect to spatial variable x.

[1] Each side corresponds to a "cutting point" in Zhu et al. (1997).

Meanwhile, let

$$\begin{aligned}\delta W = {} & f_B \delta y(0,t) + m_B \delta y'(0,t) \\ & - f_T \delta y(l,t) - m_T \delta y'(l,t)\end{aligned} \tag{3}$$

be the external work variation.

The extended Hamilton's principle yields

$$\int_{t_1}^{t_2} (\delta K - \delta V + \delta W)\, dt = 0 \tag{4}$$

for any $t_1 < t_2$. With integration by parts, it follows from (1) and (2) that

$$\begin{aligned}\int_{t_1}^{t_2} \delta K dt &= \int_{t_1}^{t_2}\int_0^l \rho \dot{y}(x,t)\delta\dot{y}(x,t) dx dt \\ &= \int_0^l \int_{t_1}^{t_2} \rho \dot{y}(x,t)\delta\dot{y}(x,t) dt dx \\ &= \int_0^l \rho \dot{y}(x,t)\delta y(x,t) \,|_{t_1}^{t_2}\, dx \\ &\quad - \int_0^l \int_{t_1}^{t_2} \rho \ddot{y}(x,t)\delta y(x,t) dt dx\end{aligned} \tag{5}$$

$$\begin{aligned}\int_{t_1}^{t_2} \delta V dt &= \int_{t_1}^{t_2}\int_0^l EIy''(x,t)\delta y''(x,t) dx dt \\ &= \int_{t_1}^{t_2} EIy''(x,t)\delta y'(x,t) \,|_0^l\, dt \\ &\quad - \int_{t_1}^{t_2}\int_0^l EIy'''(x,t)\delta y'(x,t) dx dt \\ &= \int_{t_1}^{t_2} EIy''(x,t)\delta y'(x,t) \,|_0^l\, dt \\ &\quad - \int_{t_1}^{t_2} EIy'''(x,t)\delta y(x,t) \,|_0^l\, dt \\ &\quad + \int_{t_1}^{t_2}\int_0^l EIy''''(x,t)\delta y(x,t) dx dt.\end{aligned} \tag{6}$$

Note that $\delta y(x,t) = 0$ at $t = t_1$ and $t = t_2$. Substituting (3), (5), and (6) into (4) yields the link dynamic equation

$$\rho \ddot{y}(x,t) + EIy''''(x,t) = 0 \tag{7}$$

for $x \in [0, l]$ subject to the boundary conditions

$$f_B = EIy'''(0,t) \tag{8}$$

$$m_B = -EIy''(0,t) \tag{9}$$
$$f_T = EIy'''(l,t) \tag{10}$$
$$m_T = -EIy''(l,t) \tag{11}$$

3. CONTROL AND STABILITY

3.1 Control Law

In view of (7)-(11), the link model based control is designed as

$$\rho\ddot{y}_r(x,t) + EIy_r''''(x,t) + k_v\left[\dot{y}_r(x,t) - \dot{y}(x,t)\right] = 0 \tag{12}$$

for $x \in [0,l]$ subject to the boundary conditions

$$f_{Br} = EIy_r'''(0,t) \tag{13}$$
$$m_{Br} = -EIy_r''(0,t) \tag{14}$$
$$f_{Tr} = EIy_r'''(l,t) \tag{15}$$
$$m_{Tr} = -EIy_r''(l,t) \tag{16}$$

where y_r, f_{Br}, m_{Br}, f_{Tr}, and m_{Tr} represent the required variables of y, f_B, m_B, f_T, and m_T, respectively. All required variables will be defined in the next section.

3.2 Stability Analysis

Subtracting (7) from (12) yields

$$\begin{aligned}&\rho\left[\ddot{y}_r(x,t) - \ddot{y}(x,t)\right] + EI\left[y_r''''(x,t) - y''''(x,t)\right]\\ &+k_v\left[\dot{y}_r(x,t) - \dot{y}(x,t)\right] = 0.\end{aligned} \tag{17}$$

As an important step in the VDC approach, the non-negative accompanying function of the link is chosen as

$$\nu = \nu_K + \nu_V \tag{18}$$
$$\nu_K = \frac{1}{2}\int_0^l \rho\left[\dot{y}_r(x,t) - \dot{y}(x,t)\right]^2 dx \tag{19}$$
$$\nu_V = \frac{1}{2}\int_0^l EI\left[y_r''(x,t) - \dot{y}''(x,t)\right]^2 dx. \tag{20}$$

With integration by parts, it follows from (17) and (19) that

$$\begin{aligned}\dot{\nu}_K &= \int_0^l \rho\left[\dot{y}_r(x,t) - \dot{y}(x,t)\right]\left[\ddot{y}_r(x,t) - \ddot{y}(x,t)\right] dx\\ &= -\int_0^l \left[\dot{y}_r(x,t) - \dot{y}(x,t)\right]\\ &\qquad \times EI\left[y_r''''(x,t) - y''''(x,t)\right] dx\\ &\quad -\int_0^l k_v\left[\dot{y}_r(x,t) - \dot{y}(x,t)\right]^2 dx\\ &= -\left[\dot{y}_r(x,t) - \dot{y}(x,t)\right] EI\left[y_r'''(x,t) - y'''(x,t)\right]\Big|_0^l\\ &\quad +\int_0^l \left[\dot{y}_r'(x,t) - \dot{y}'(x,t)\right]\\ &\qquad \times EI\left[y_r'''(x,t) - y'''(x,t)\right] dx\\ &\quad -\int_0^l k_v\left[\dot{y}_r(x,t) - \dot{y}(x,t)\right]^2 dx\\ &= -\left[\dot{y}_r(x,t) - \dot{y}(x,t)\right] EI\left[y_r'''(x,t) - y'''(x,t)\right]\Big|_0^l\\ &\quad +\left[\dot{y}_r'(x,t) - \dot{y}'(x,t)\right] EI\left[y_r''(x,t) - y''(x,t)\right]\Big|_0^l\\ &\quad -\int_0^l \left[\dot{y}_r''(x,t) - \dot{y}''(x,t)\right]\\ &\qquad \times EI\left[y_r''(x,t) - y''(x,t)\right] dx\\ &\quad -\int_0^l k_v\left[\dot{y}_r(x,t) - \dot{y}(x,t)\right]^2 dx.\end{aligned} \tag{21}$$

Substituting (21) and the time derivative of (19) into the time derivative of (18) yields

$$\begin{aligned}\dot{\nu} = &-\int_0^l k_v\left[\dot{y}_r(x,t) - \dot{y}(x,t)\right]^2 dx\\ &+p_B - p_T\end{aligned} \tag{22}$$

where

$$\begin{aligned}p_B &= \left[\dot{y}_r(0,t) - \dot{y}(0,t)\right] EI\left[y_r'''(0,t) - y'''(0,t)\right]\\ &\quad -\left[\dot{y}_r'(0,t) - \dot{y}'(0,t)\right] EI\left[y_r''(0,t) - y''(0,t)\right]\\ &= \left[\dot{y}_r(0,t) - \dot{y}(0,t)\right]\left(f_{Br} - f_B\right)\\ &\quad +\left[\dot{y}_r'(0,t) - \dot{y}'(0,t)\right]\left(m_{Br} - m_B\right)\end{aligned} \tag{23}$$

$$\begin{aligned}p_T &= \left[\dot{y}_r(l,t) - \dot{y}(l,t)\right] EI\left[y_r'''(l,t) - y'''(l,t)\right]\\ &\quad -\left[\dot{y}_r'(l,t) - \dot{y}'(l,t)\right] EI\left[y_r''(l,t) - y''(l,t)\right]\\ &= \left[\dot{y}_r(l,t) - \dot{y}(l,t)\right]\left(f_{Tr} - f_T\right)\\ &\quad +\left[\dot{y}_r'(l,t) - \dot{y}'(l,t)\right]\left(m_{Tr} - m_T\right)\end{aligned} \tag{24}$$

in view of (8)-(11) and (13)-(16).

In view of the VDC approach, equation (22) gives the exact form needed for guaranteeing the stability of the entire robot. Both p_B and p_T defined by (23) and (24) represent the *virtual power flows* at the two ends of the link. A *virtual power flow* is an inner product of the linear and angular velocity errors and the force and moment errors. At the end, all *virtual power flows* of a system can be canceled out (in the time derivative of the summation of all non-negative accompanying functions) to guarantee the L_2 and L_∞ stability of the entire robot, see Zhu et al. (1997).

3.3 Alternative Use of Virtual Power Flows

In a particular case that the force and moment at point T are measurable and the force and moment at point B are controllable, the following design

$$f_{Tr} = f_T + k_{fT}\left[\dot{y}_r(l,t) - \dot{y}(l,t)\right] \tag{25}$$
$$m_{Tr} = m_T + k_{mT}\left[\dot{y}_r'(l,t) - \dot{y}'(l,t)\right] \tag{26}$$
$$f_B = f_{Br} + k_{fB}\left[\dot{y}_r(0,t) - \dot{y}(0,t)\right] \tag{27}$$
$$m_B = m_{Br} + k_{mB}\left[\dot{y}_r'(0,t) - \dot{y}'(0,t)\right] \tag{28}$$

makes

$$\begin{aligned}\dot{\nu} = &-\int_0^l k_v \left[\dot{y}_r(x,t) - \dot{y}(x,t)\right]^2 dx \\ &-k_{fB}\left[\dot{y}_r(0,t) - \dot{y}(0,t)\right]^2 \\ &-k_{mB}\left[\dot{y}'_r(0,t) - \dot{y}'(0,t)\right]^2 \\ &-k_{fT}\left[\dot{y}_r(l,t) - \dot{y}(l,t)\right]^2 \\ &-k_{mT}\left[\dot{y}'_r(l,t) - \dot{y}'(l,t)\right]^2. \end{aligned} \quad (29)$$

It follows from $\nu \geq 0$ that

$$\dot{y}_r(0,t) - \dot{y}(0,t) \in L_2 \quad (30)$$
$$\dot{y}'_r(0,t) - \dot{y}'(0,t) \in L_2 \quad (31)$$
$$\dot{y}_r(l,t) - \dot{y}(l,t) \in L_2 \quad (32)$$
$$\dot{y}'_r(l,t) - \dot{y}'(l,t) \in L_2. \quad (33)$$

With bounded reference signals and their time derivatives, the flexibility of the link ensures the continuity of the states. It further leads to the asymptotic stability

$$\dot{y}_r(0,t) - \dot{y}(0,t) \to 0 \quad (34)$$
$$\dot{y}'_r(0,t) - \dot{y}'(0,t) \to 0 \quad (35)$$
$$\dot{y}_r(l,t) - \dot{y}(l,t) \to 0 \quad (36)$$
$$\dot{y}'_r(l,t) - \dot{y}'(l,t) \to 0. \quad (37)$$

4. CONTROL IMPLEMENTATION

In this section, implementation of the control law formed by (12)-(16) is addressed.

In the standard VDC approach, the control algorithm is to find f_{Br} and m_{Br} from given f_{Tr} and m_{Tr}. This process corresponds to finding $y_r(0,t)$, $y'_r(0,t)$, $y''_r(0,t)$, and $y'''_r(0,t)$ from given $y_r(l,t)$, $y'_r(l,t)$, $y''_r(l,t)$, and $y'''_r(l,t)$ subject to the constraint equation (12), since $y''_r(0,t)$ and $y'''_r(0,t)$ give f_{Br} and m_{Br} from (13) and (14) and f_{Tr} and m_{Tr} give $y'''_r(l,t)$ and $y''_r(l,t)$ from (15) and (16). The variables $y_r(l,t)$, $y'_r(l,t)$ are determined from motion control specification.

In the control implementation, the link is divided into $N > 0$ discrete sections with $x(0) = 0$ and $x(N) = l$.

Backward differentiation is applied to both time and spatial variables. It follows that

$$\dot{y}(x,k) = \frac{y(x,k) - y(x,k-1)}{\Delta T} \quad (38)$$
$$y'(x(j),t) = \frac{y(x(j),t) - y(x(j-1),t)}{\Delta x} \quad (39)$$

where ΔT is the sampling time of the control system with k being a positive integer and $\Delta x = l/N$ is the length of a discrete section with $j \in \{1, N\}$.

The overall computational algorithm is as follows:

Step 1: For given $\ddot{y}_r(l,k)$, compute

$$y''''_r(l,k) = -\frac{\rho \ddot{y}_r(l,k) + k_v\left[\dot{y}_r(l,k) - \dot{y}(l,k)\right]}{EI} \quad (40)$$

from (12).

Step 2: For given $y_r(l,k)$, $y'_r(l,k)$, $y''_r(l,k)$, $y'''_r(l,k)$, and $y''''_r(l,k)$, compute

$$y'''_r(x(N-1),k) = y'''_r(x(N),k) - \Delta x y''''_r(x(N),k) \quad (41)$$
$$y''_r(x(N-1),k) = y''_r(x(N),k) - \Delta x y'''_r(x(N),k) \quad (42)$$
$$y'_r(x(N-1),k) = y'_r(x(N),k) - \Delta x y''_r(x(N),k) \quad (43)$$
$$y_r(x(N-1),k) = y_r(x(N),k) - \Delta x y'_r(x(N),k). \quad (44)$$

Step 3: The required velocity and acceleration at $x(N-1)$ are updated by

$$\dot{y}_r(x(N-1),k) = \frac{y_r(x(N-1),k) - y_r(x(N-1),k-1)}{\Delta T} \quad (45)$$
$$\ddot{y}_r(x(N-1),k) = \frac{\dot{y}_r(x(N-1),k) - \dot{y}_r(x(N-1),k-1)}{\Delta T}. \quad (46)$$

Step 4: Repeat Step 1 to Step 3 iteratively from $x(N-1)$ to $x(0)$ to obtain $y_r(0,k)$, $y'_r(0,k)$, $y''_r(0,k)$, $y'''_r(0,k)$, and further f_{Br} and m_{Br} from (13) and (14).

In some applications, the linear or angular position at point B may be subject to constraints, such as $y(0,t) = 0$ for a link mounted on a motor rotor or $y'(0,t) = 0$ when only linear motion is permitted. In such a case, the corresponding required variable at point T has to be released by adding a constant. For instance, if $y_r(0,t) = y(0,t) = 0$ is required, then $y_r(l,t)$ has to be released; or if $y'_r(0,t) = y'(0,t) = 0$ is required, then $y'_r(l,t)$ has to be released.

5. SIMULATIONS

Simulations are carried out to verify the validity of the control developed in the previous sections.

It is assumed that the link as illustrated in Fig. 1 has a free end at point T (excluding motion in x axis), which makes $f_T = 0$ and $m_T = 0$, and has both force (in y axis) and moment controlled at point B, which makes f_B and m_B to be control variables. Furthermore, it is assumed that only the positions and angles at both ends, denoted as $y(0,t)$, $y'(0,t)$, $y(l,t)$, and $y'(l,t)$, are measurable. Thus, $k_v = 0$ is used in (12), since $\dot{y}(x,t)$ for $x \in (0,l)$ is not available.

The control objective is to make the tip position $y(l,t)$ track its desired variable $y_d(l,t)$, while maintaining the orientation as $y'(l,t) \to 0$. To serve the purpose, the required linear and angular velocities at point T are designed as

$$\dot{y}_r(l,t) = \dot{y}_d(l,t) + \lambda_f\left[y_d(l,t) - y(l,t)\right] \quad (47)$$
$$\dot{y}'_r(l,t) = -\lambda_m y'(l,t) \quad (48)$$

where $\lambda_f > 0$ and $\lambda_m > 0$ are two control parameters. Subsequently, the boundary control conditions (25)-(28) are modified to

$$\begin{aligned} f_{Tr} = &\, k_{fv}\left[\dot{y}_r(l,t) - \dot{y}(l,t)\right] \\ &+ k_{fI}\int_0^t \left[\dot{y}_r(l,t) - \dot{y}(l,t)\right] dt \end{aligned} \quad (49)$$

Table 1. Simulation systems and control parameters

	System I	System II
ρ (kg/m)	0.95	11.8
EI (Nm^2)	500	1.08×10^7
l (m)	1.5	6.8
λ_f (1/s)	0.1	0.5
k_{fv} (Ns/m)	0.001	10.8
k_{fI} (N/m)	0.01	0.108
λ_m (1/s)	0.1	0.5
k_{mv} (Nms)	5.7×10^{-5}	0.618
k_{mI} (Nm)	0.057	6.19×10^3
k_{fB} (Ns/m)	5	216
k_{mB} (Nms)	2.5	1.08×10^3

$$m_{Tr} = k_{mv}\left[\dot{y}_r'(l,t) - \dot{y}'(l,t)\right] + k_{mI}\int_0^t \left[\dot{y}_r'(l,t) - \dot{y}'(l,t)\right] dt \quad (50)$$

$$f_B = f_{Br} + k_{fB}\left[\dot{y}_r(0,t) - \dot{y}(0,t)\right] \quad (51)$$

$$m_B = m_{Br} + k_{mB}\left[\dot{y}_r'(0,t) - \dot{y}'(0,t)\right] \quad (52)$$

where $k_{fv} > 0$, $k_{fI} > 0$, $k_{mv} > 0$, $k_{mI} > 0$, $k_{fB} > 0$, and $k_{mB} > 0$ are six control parameters. Comparing (25) and (26) with (49) and (50) reveals that an integration term is added to the right hand sides of (49) and (50), respectively, to eliminate steady state errors. The addition of the integration terms does not affect the stability result. Simply adding

$$\frac{1}{2}k_{fI}\left(\int_0^t \left[\dot{y}_r(l,t) - \dot{y}(l,t)\right] dt\right)^2 + \frac{1}{2}k_{mI}\left(\int_0^t \left[\dot{y}_r'(l,t) - \dot{y}'(l,t)\right] dt\right)^2$$

to the right hand side of (18) ensures the same stability results (30)-(37). Substituting (47) and (48) into (36) and (37) yields

$$\dot{y}_d(l,t) - \dot{y}(l,t) \to 0 \quad (53)$$

$$y_d(l,t) - y(l,t) \to 0 \quad (54)$$

$$\dot{y}'(l,t) \to 0 \quad (55)$$

$$y'(l,t) \to 0. \quad (56)$$

Two sets of parameters getting from two typical space systems are used in the simulations. The system parameters together with corresponding control parameters are listed in Table 1. Meanwhile, $N = 100$ and $\Delta T = 0.001$ (s) are used in control implementation.

The simulation results are illustrated in Figs. 2 to 7. Figs. 2 to 4 illustrate the tip position tracking result $y_d(l,t) - y(l,t)$, the tip angle $y'(l,t)$, and the base control force and moment f_B and m_B, respectively, for a more flexible system. The simulation results for a more rigid system are illustrated in Figs. 5 to 7.

The link model used in the simulations is an ideal flexible beam without imposing damping. However, the simulation results demonstrate very smooth responses without showing oscillation phenomenon. This is one of the advantages

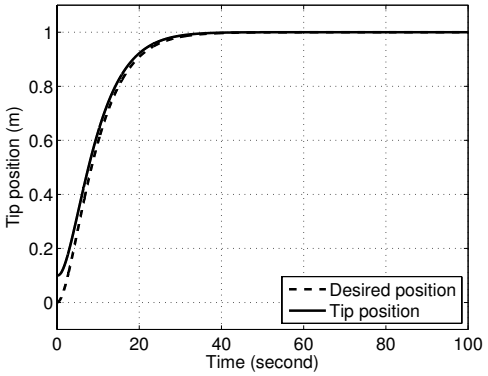

Fig. 2. Tip position tracking result for System I.

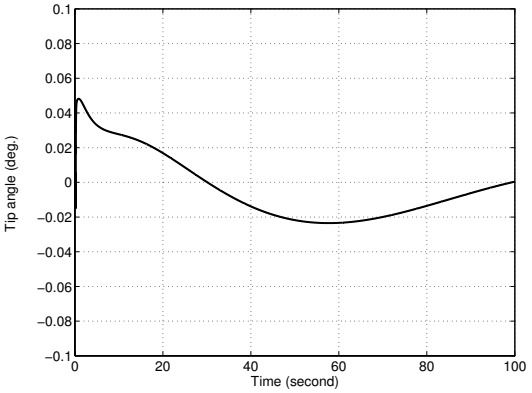

Fig. 3. Tip angle for System I.

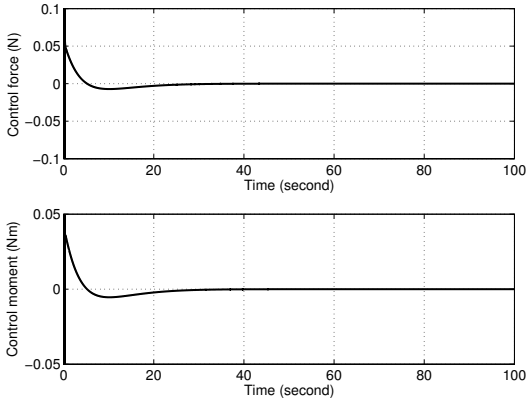

Fig. 4. Control force and moment at point B for System I.

of using the VDC approach that brings in active damping to the system and guarantees asymptotic control for designed positions and velocities.

For different applications, only the eight control parameters outlined in Table 1 need to be changed.

It is worth noting that the proposed VDC approach is quite robust against link stiffness. It has been successfully applied to two simulated systems with a stiffness difference of more than *four* orders of magnitude.

6. CONCLUSION

In this paper, the *virtual decomposition control* approach has been applied to planar flexible link robots for the first

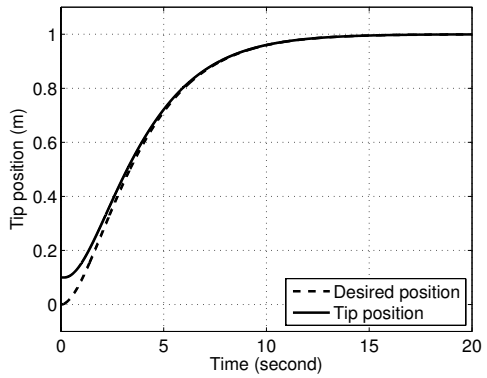

Fig. 5. Tip position tracking result for System II.

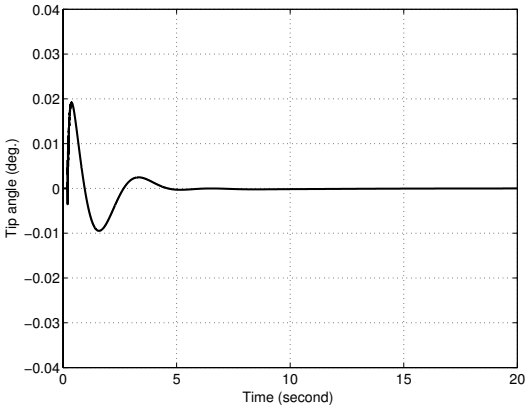

Fig. 6. Tip angle for System II.

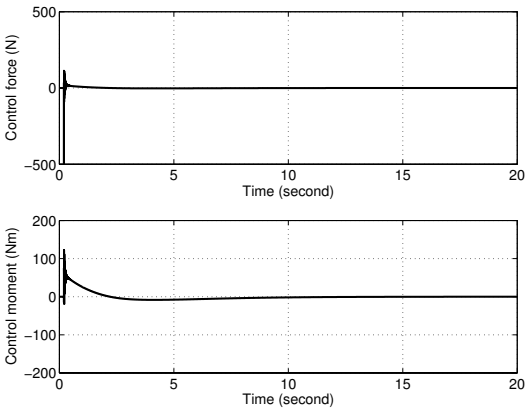

Fig. 7. Control force and moment at point B for System II.

time. Unlike other approaches, the VDC approach only needs the dynamics of individual links for control computation, while guaranteeing the stability and convergence of the entire robot. Technically, the dynamic interactions between an individual link and the rest of the system are rigorously represented by two *virtual power flows* (at the two virtual "cutting points" of the link) appeared in the time derivative of the corresponding non-negative accompanying function. Since the two *virtual power flows* have different signs, all *virtual power flows* of the entire robot are to be canceled out to ensure the stability. This approach has been tested on two simulated systems with a substantial stiffness difference of more than $four$ orders of magnitude. The responses are smooth without showing oscillation phenomenon as usually happened when no damping is presented in the link model.

Finally, it is worth noting that the *virtual decomposition control* is naturally applicable to the control problem of multiple flexible-link robots in 3D, despite a planar flexible link robot is treated in this paper for simplicity. Regardless of the complexity of a flexible robot, the dynamics needed for implementing VDC include only the dynamics of individual links and of the joints. Therefore, the VDC approach opens the door to dynamics-based control of complex flexible-link robots, at least in theory. Future research will focus on simulations and experiments of more general and realistic flexible robots.

REFERENCES

A. De Luca and B. Siciliano. Inversion-based nonlinear control of robot arms with flexible links. *AIAA J. Guidance, Control, and Dynamics*, vol. 16(6):1169–1176, 1993.

J.L. Junkins and Y. Kim,. *Introduction to Dynamics and Control of Flexible Structures*. AIAA Education Series, Washington DC, 1993.

H. Kanoh, S. Tzafestas, H.G. Lee, and J. Kalat. Modelling and control of flexible robot arms. *25th IEEE Conference on Decision and Control*, 25:1866–1870, 1986.

S.E. Khadem and A.A. Pirmohammadi. Analytical development of dynamic equations of motion for a three-dimensional flexible link manipulator with revolute and prismatic joints. *IEEE Trans. Syst., Man, Cybern., B, Cybern.*, 33(2):237–249, Apr. 2003.

Z.H. Luo. Direct strain feedback control of flexible robot arms: new theoretical and experimental results. *IEEE Trans. Automat. Contr.*, 38(11):1610–1622, 1993.

Z.H. Luo, B.Z. Guo, and O. Morgul. *Stability and Stabilization of Infinite Dimensional Systems with Applications*. London, U.K., Springer-Verlag, 1999.

A. Macchelli, C. Melchiorri, and S. Stramigioli. Port-based modeling of a flexible link. *IEEE Trans. Robot. and Automat.*, 23(4):650–660, 2007.

M.S. de Queiroz, D.M. Dawson, M. Agarwal, and F. Zhang. Adaptive nonlinear boundary control of a flexible link robot arm. *IEEE Trans. Robot. Automat.*, 15(4):779-787, 1999.

J.A. Somolinos, V. Feliu, and L. Snchez. Design, dynamic modelling and experimental validation of a new three-degree-of-freedom flexible arm. *Mechatronics*, 12(7):919-948, 2002.

D. Wang and M. Vidyasagar. Modeling a class of multilink manipulators with the last link flexible. *IEEE Trans. Robot. Automat.*, 8(1):33-41, Feb. 1992.

W.-H. Zhu, Y.-G. Xi, Z.-J. Zhang, Z. Bien, and J. De Schutter. Virtual decomposition based control for generalized high dimensional robotic systems with complicated structure. *IEEE Trans. Robot. and Automat.*, 13(3):411-436, 1997.